IOP Conf. Series: Materials Science and Engineering **399** (2018) 012017 doi:10.1088/1757-899X/399/1/012017

Hybrid modelling for thermal deformation prediction of high speed motorized spindle

L T Fan[1,2], X R Jing[1], L X Zhang[1,2] and D Li[1,2*]

[1] School of Mechanical Engineering, Shenyang Jianzhu University, Shenyang 110168, China
[2] National-Local Joint Engineering Laboratory of NC Machining Equipment and Technology of High-Grade Stone, Shenyang Jianzhu University, Shenyang 110168, China

[*] E-mail: lidong@sjzu.edu.cn

Abstract. Thermal-induced deformation accounts for 40-70% of the total dimensional and shape errors that arise from various sources of machine tools. This paper suggests a hybrid model based on regression-based analysis and computation-based simulation to predict the thermal deformation of high speed motorized spindle. COMSOL Multiphysics was used to obtain the numerical solutions of the thermal deformation, and the PLS algorithm was used to modify the error between the simulation model and the experimental data collected from the spindle test system. The experimental results showed that the proposed hybrid model could predict thermal deformation effectively and accurately, and it can be used for real-time thermal deformation compensation to improve the machining accuracy of NC machine tool.

1. Introduction

Thermal-induced deformation accounts for 40 - 70% of the total dimensional and shape errors that arise from various sources of machine tools [1-3]. Thermal issues in machine tools have been studied extensively in the past decades, and detailed reviews can be found in literatures [4-11]. In order to improve the machining accuracy of finished parts, effective thermal error compensation measures are achieved via re-adjusting the axes positioning or via shifting the original coordinates based on the thermal deformation model.

In order to estimate thermal deformation, either computation-based or regression-based models are employed [12-24]. The computation-based models can be represented with thermal transfer functions. The finite element method (FEM) and finite difference method are widely used to model the thermal behaviour of motorized spindle under the influence of heat sources inside the structure and in its surroundings. Numerous computational models have been proposed as summarized in the literatures [25-31]. However, due to the low efficiency, the computation-based models were rarely employed in online thermal compensation, usually used only for simulation analysis and providing a design reference. As for regression-based models, the relationships between temperature rise and thermal deformation are studied based on the measured data. The regression-based models mainly include multivariate statistical models [19], neural network models [21], and gray theoretical models [22]. All the regression-based models play an important role in the thermal error compensation implementation. However, the accuracy of the data model depends on the quantity and quality of the modelling data.

Once the data exceeds the scope of modelling data, the model predictions could show a serious deviation, that is, weak generalization ability. Hybrid modelling can achieve the best of both computation-based and regression-based models. Combining computational analysis with experimental data, regression analysis is used to extract complex information that cannot be explained by the computation-based model, and the computation-based model could improve the generalization ability of the regression-based model.

This paper proposes a hybrid model based on PLS and COMSOL to predict the thermal deformation of the high-speed motorized spindle. Firstly, through the analysis of the temperature field of the motorized spindle, the geometric model and thermal boundary conditions for finite element modelling were obtained. The COMSOL Multiphysics software was used to simulate the motorized spindle to obtain the thermal deformation in three dimensions. Then, the PLS regression method was used to establish the relationship between the temperature rise and the errors of COMSOL model. Experimental data collected from the spindle thermal deformation test system were used for the model validation.

2. Thermal characteristics of motorized spindle

The structure of the motorized spindle is shown in figure 1, which includes the house, stator and rotor of the motor, shaft, coolant jacket and bearing set. In general, the motorized spindle is equipped with a built-in motor as an integrated component. The thermal deformation is induced by the electromagnetic loss between the stator and the rotor, and mechanical friction loss was generated in the bearing set. All the energy loss is converted into heat and then transferred to the shaft, leading to thermal deformation, especially in the axial direction, which heavily influences the machining accuracy.

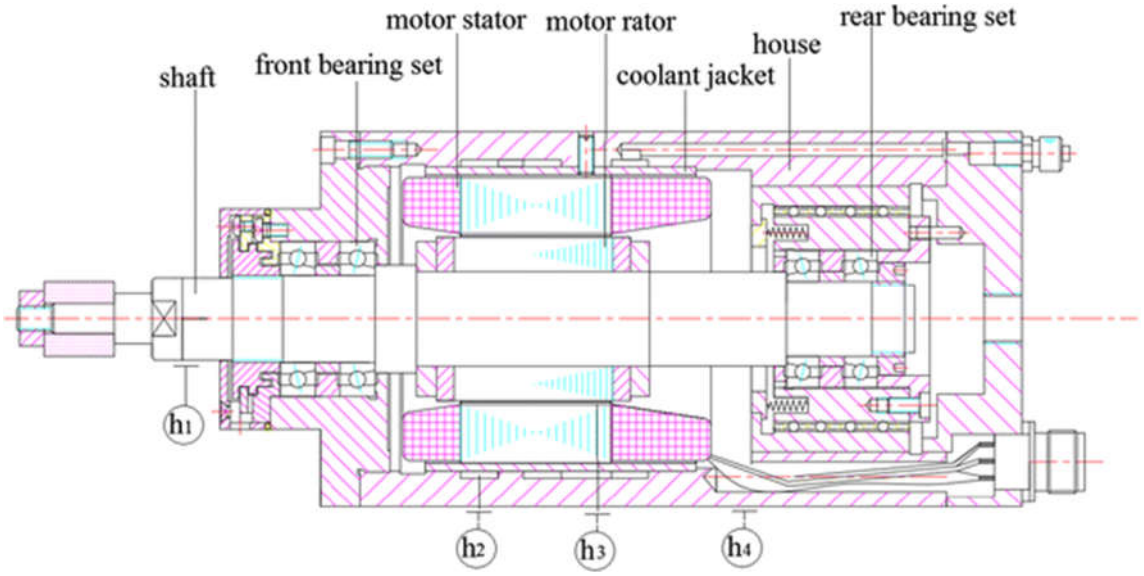

Figure 1. The structure of motorized spindle.

According to the energy conservation law:

$$\rho_1 C_{P1} \frac{\partial T}{\partial t} - \nabla \cdot (k \nabla T) = \Omega, \tag{1}$$

where $\Omega = \frac{Q}{V}$ is the heat generation rate ($W \cdot m^{-3}$), Q is the heat source (W), V is the volume of the heat source (m^3), ρ_1 is the density ($kg \cdot m^{-3}$), C_{P1} is the heat capacity ($J \cdot kg^{-1} \cdot K^{-1}$), T is the temperature (K), k is the thermal conductivity ($W \cdot m^{-1} \cdot K^{-1}$).

The thermal deformation equation of the spindle is:

$$\varepsilon_{th} = \alpha(T)(T - T_{ref}), \tag{2}$$

where ε_{th} is the thermal strain, α is the thermal deformation coefficient (1/K), T_{ref} is the ambient temperature (K).

The stator in the motorized spindle is cooled by water in the coolant jacket, and the rotors and bearings are cooled by compressed air in the oil mist lubrication device. **As** shown in figure 1, it is assumed that there are forced convection heat transfer in the air-gaps that between the stator and rotor, the rotor and the compressed air, the cooling water and the water jacket. There is natural convection heat transfer between the shell surface and environment air. For the convective heat transfer, according to Newton's Law, the relationship between the heat flow vector and the heat transfer coefficient is

$$q = h \cdot (T - T_{ref}), \tag{3}$$

where h is the heat transfers coefficient ($W \cdot m^{-2} \cdot K^{-1}$), q is the heat flux ($J \cdot m^{-2} \cdot s^{-1}$).

A finite element model can be established to predict the thermal deformation of the motorized spindle taking into account the structural parameters and operating condition based on the above equations.

3. Computation model based on COMSOL

The finite element model is obtained based on figure 1 by assuming that the bearing, the rotor and the stator are simplified to be assembled on the shaft, ignoring all the screws, the vent holes, the through holes, and integrating the fine structure, the bearing inner ring, outer ring and rolling elements. Because the motorized spindle is an axial symmetrical structure, 1/4 of the finite element model of motorized spindle is shown in figure 2. The total simulation time is 4800 seconds, and the step size is 300 seconds. A tetrahedral mesh structure of free partition is used and refined with 125,626 tetrahedral elements, 23,087 triangular elements, and 2,339 edge units. The material properties of the model are shown in table 1.

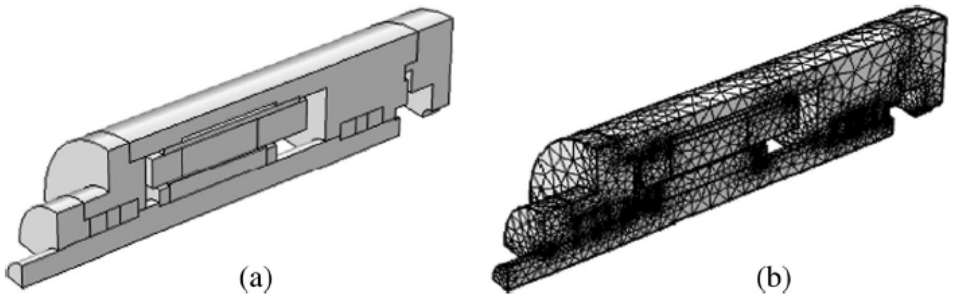

Figure 2. The finite element model of motorized spindle (a) geometrical model (b) meshing model.

The boundary conditions involve the stator heat, rotor heat and bearing heat obtained by the power loss test. In addition, there are four obvious different heat transfer processes of the 150MD24Z7.5 motorized spindle as shown in table 2, refer to figure 1. Therefore, the heat transfer coefficient between the shaft end and the environment air is h_1, the heat transfer coefficient between the air-gap and compressed air is h_2, the heat transfer coefficient between the cool water and the coolant jacket is h_3, and the heat transfer coefficient between the shell surface and environment air is h_4. The stator losses, rotor losses and bearing friction losses of the motorized spindle are obtained by the experimental method under the speed of 5,000 *rpm*, 8,000 *rpm*, 10,000 *rpm* and 12,000 *rpm*. The values of h_1~h_4 are listed in table 3.

The finite element method is used to obtain the numerical solutions to the temperature and thermal errors. The temperature field distribution of the motorized spindle system is shown in figure 3. The maximum temperature area distributes mainly over the rotor and the shaft core. The reasons are that the rotor accounts for one third of the motor heat dissipation, and there is no cool system to directly take out the heat of the rotor and the shaft core. The temperature field of the stator is lower than that of the rotor because the spindle sleeve connecting with the stator has a cool system which can greatly decrease the temperature of the stator and the spindle sleeve.

Table 1. Material properties for FEM.

	Material	Density (kg/m^3)	Linear expansion coefficient ($10^{-6}K^{-1}$)	Modulus of elasticity (Gpa)	Poisson ratio	Heat capacity J/(Kg·K)	Thermal conductivity W/(m·K)
Stator	Silicon steel	7.82	13	198	0.26	535	35
35Rotor	Cast aluminum	2.77	23.6	69	0.32	875	167
Winding	Copper	8.933	17	80	0.36	385	400
Bearing and other	Steel	7.872	10	208	0.3	434	60.5

Table 2. Heat transfer process of motorized spindle.

Numbering	position
h_1	Forced convective heat transfer between the shaft end and the environment air
h_2	Forced convection heat transfer between the air-gap and compressed air
h_3	Forced convection heat transfer between the cooling water and the coolant jacket
h_4	Natural convection heat transfer between the house surface and environment air

Table 3. Boundary conditions for FEM.

Speed(rpm)				Simulation conditions
5000	8000	10000	12000	
108.3	116	140.7	156.9	Stator heat
54.1	58	70.3	78.5	Rotor heat
2.3	17	28.7	41.3	Bearing heat
83.21	97.83	106.1	115	h_1
109.92	131.64	143.9	156.13	h_2
279	279	279	279	h_3
9.7	9.7	9.7	9.7	h_4

After the analysis of stable heat conduction has been completed, the element type is changed, the elastic module, poisons ratio and coefficient of thermal expansion are set, the analysis results of stable heat conduction serve as the temperature condition, and the DO constraints are attached to the bottom of the spindle. The results of thermal deformation analysis can be seen in figure 4.

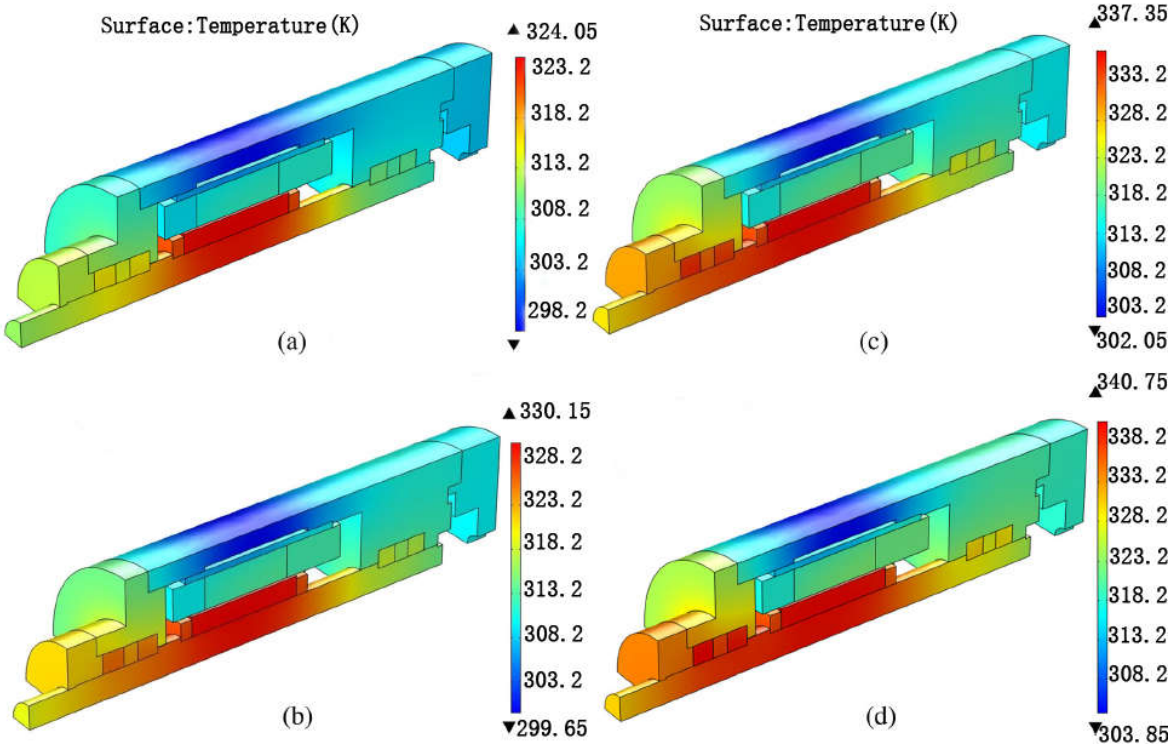

Figure 3. Temperature field distribution results (a) n=5000*rpm* (b) n=8000*rpm* (c) n=10000*rpm* (d)n=12000*rpm.*

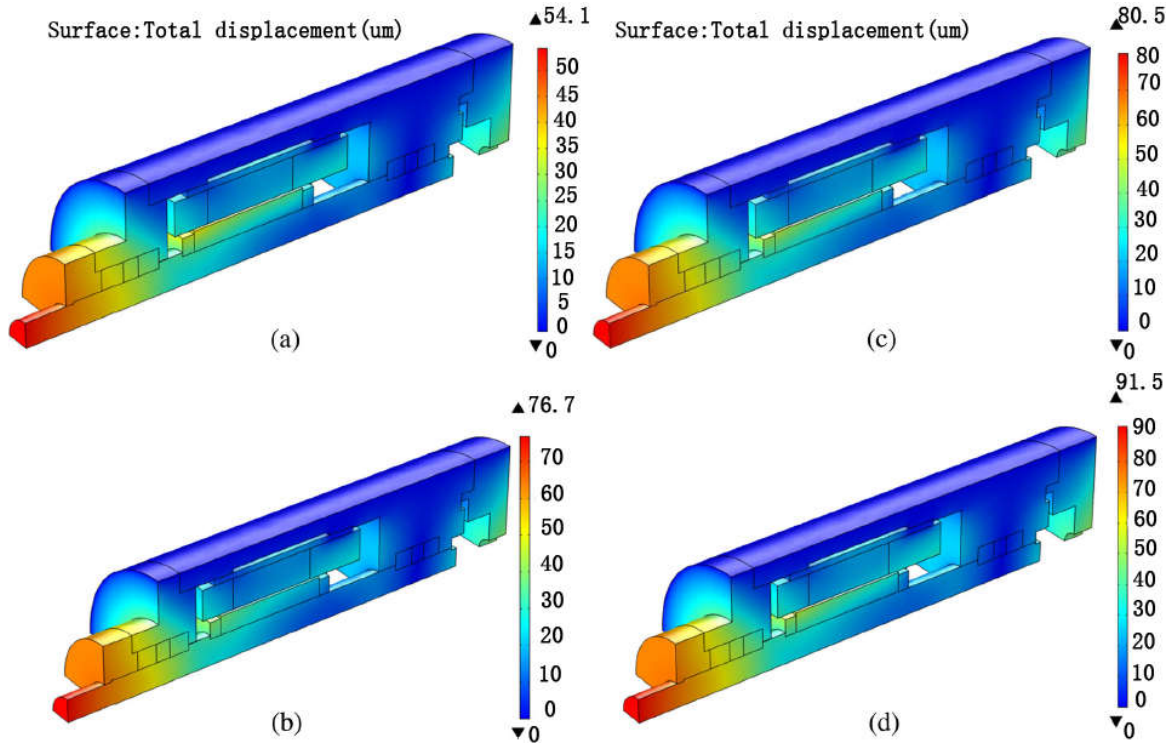

Figure 4. Thermal deformation prediction results (a) n=5000*rpm* (b) n=8000*rpm* (c) n=10000*rpm* (d)n=12000*rpm.*

The thermal deformations of the main components of the motorized spindle system are affected by the thermal characteristics and temperature field distribution, which causes the thermal error of the shaft and whole motorized spindle. In figure 4, in the axial direction, namely the Z direction, the maximum deformation is about 58*μm*, 70.4 *μm*, 72.7 *μm* and 89.6 *μm* when the speed is 5000 rpm, 8000 *rpm*, 10000 *rpm* and 12000 *rpm*, respectively. The axial deformation of the spindle is higher than the radial deformations.

The numerical solutions can approximate the analytical solutions very well as long as the spindle is correctly and finely meshed. The reliability of simulation results also depends on whether the thermal loads and boundary conditions are well defined. The accurate calculation of the thermal boundary conditions is a necessary condition for ensuring the accuracy of the finite element theory model. The inaccuracy of any of the material properties in the boundary conditions, the convection coefficient, the thermal contact resistance, and the heat generated by the heat source may cause inaccurate predictions. Moreover, the calculation process of the finite element model is relatively complex, generally requires loop iteration, and there is a case of non-convergence. Therefore, it is difficult to directly apply the thermal error compensation process. However, the finite element model describes the process of thermal deformation from the thermal characteristic mechanism. Therefore, the model has good generalization ability. Even if the operating conditions vary within a relatively wide range, the predictive result of thermal deformation can be obtained with limited accuracy. In order to improve the prediction accuracy of the model, the regression model can be used to supplement or modify the computation model. The regression model is a statistical model based on experimentally measured thermal deformation and the temperature measurement data of the motorized spindle. But the variation in the temperature measurement point of the motor spindle is similar, so there is a strong correlation problem in the data. Directly using the measurement data onto multiple regression modelling will inevitably produce multiple correlation problems. The existence of multiple correlations can seriously jeopardize the parameter estimation of the model, enlarge the model error, and destroy the stability of the model. However, the partial least-squares regression method can effectively overcome the adverse effects of multiple correlations in the model.

4. Regression model based on PLS

Partial least-squares regression is a new multivariate statistical data analysis method that integrates the basic functions of multiple linear regression analysis, canonical correlation analysis, and principal component analysis. It combines the modelling and forecasting data analysis method of the non-model data recognition analysis method and achieves the simplification of the data structure while modelling. The PLS method no longer directly considers the regression modelling of the dependent variable *Y* and the independent variable *X*. Instead, the information about the variable system is comprehensively screened again, and several new synthetic variables (principal components) that have the best explanatory power for the system are selected for regression modelling. It can effectively filter out the information overlap caused by multiple correlations and improve the accuracy of system modelling.

The PLS model consists of two parts: external relations and internal relations. There are l dependent variables $\{y_1, \cdots, y_l\}$ and m independent variables $\{x_1, \cdots, x_m\}$. Based on the n sets of observed data, the dependent variable matrix $Y_{n\times l}$ and the independent variable matrix $X_{n\times m}$ are constructed. According to the PLS algorithm, the principal components are extracted and X and Y are decomposed to get the external relation model:

$$X = TP^T + E = \sum_{i=1}^{T} t_t p_t^T + E \,, \tag{4}$$

$$Y = UQ^T + F = \sum_{i=1}^{r} u_i q_t^T + F \,, \tag{5}$$

where $P_{m\times r}$ and $Q_{1\times r}$ are the load matrices for X and Y, respectively, and $E_{n\times m}$ and $F_{n\times 1}$ are the residual matrices for X and Y, respectively. The matrices $T = [t_1, \cdots, t_r]$ and $U = [u_1, \cdots, u_r]$ are the score matrices of the matrices *X* and *Y*, respectively, where the elements $t_1, \cdots, t_r$ and $u_1, \cdots, u_r$ are the extracted principal components.

The external relational model guarantees that T and U represent the data tables X and Y as closely as possible. The internal relational model ensures that the principal component T of the independent variable has the strongest explanatory power for the principal component U of the dependent variable. Therefore, the following regression model can be established for the principal components:

$$U = TB + R, \tag{6}$$

where $B = diag\{b_1 \cdots b_r\}$ is the regression factor matrix and R is the U residual matrix. The regression coefficients in the PLS model can be calculated by nonlinear iteration or using singular value decomposition.

As a regression model, the accuracy of the PLS model depends on the quantity and quality of the modelling data. Therefore, if the measurement data are inaccurate, or if the model prediction exceeds the range of modelling data, the model prediction results will be inaccurate. This means that the application scope of the PLS model will be limited by the capacity of the modelling data, and the generalization ability of the PLS model will be poor.

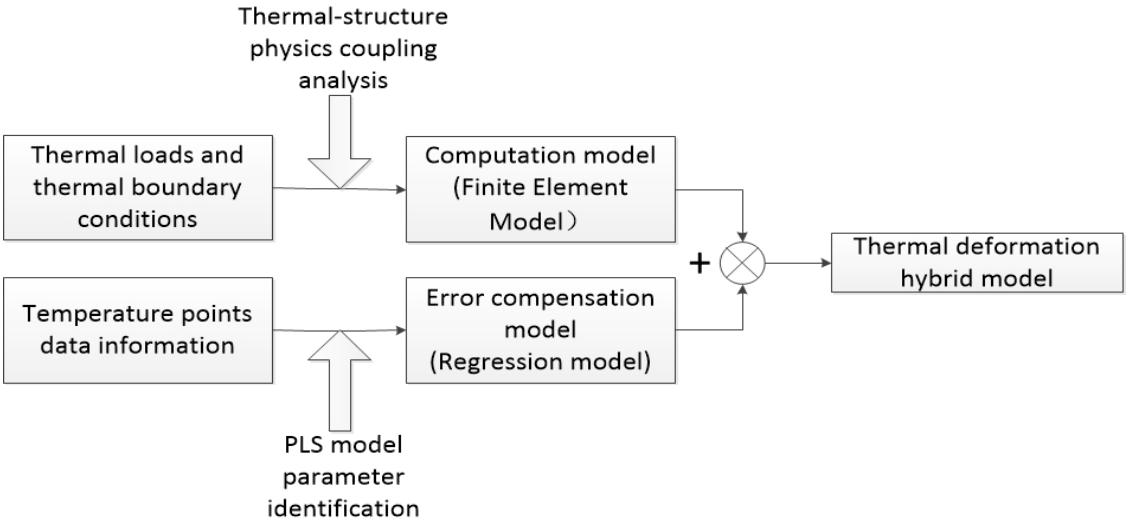

Figure 5. Structure of the thermal deformation hybrid model.

5. Thermal deformation prediction based on hybrid modelling method

The mixed use of computation models and regression models can achieve the effect of complementing each other. The PLS-based regression model can extract unexplained internal complex information from the computation model. And the computation model based on the finite element can provide the prior knowledge of thermal deformation and improve the generalization ability of the regression model. Based on the above design concept, the design framework of the thermal deformation hybrid model of the high-speed motorized spindle is shown in figure 5. The overall model consists of a finite element model and an error compensation model. The PLS method is used to predict the thermal deformation error between the output of the finite element model and the experimental data. Next, the output of the finite element model and the error compensation model are superimposed to obtain a hybrid model of thermal deformation. The hybrid model effectively combines the merits of the

computation model and the regression model. Using the finite element model as the basis of the hybrid model, the extrapolation and generalization capabilities of the model have been improved, and the PLS model has been used to make up for the computational error, which has greatly improved the prediction results of the thermal deformation model.

The specific steps for the establishment of the thermal deformation hybrid model are as follows:

- Based on the heat loss experiment, the heat transfers coefficients and thermal loads calculated at different speeds of the motorized spindle are loaded as boundary conditions into the spindle model. According to the thermal stress analysis, the computation model of thermal deformation of the high-speed motorized spindle during thermal steady state is obtained.
- A regression model is established based on experimental data collected at different speeds. The input of the model is the temperature rise of each temperature measuring point, and the output of the model is the error between the experimental data and the computation results from the finite element model.
- After calculating the cross-validation, the principal components for regression modelling is selected, the principal component regression model is reduced to the original variable, and the thermal deformation error compensation model based on the PLS method is obtained.
- The performance of the thermal deformation hybrid model is evaluated based on the experimental data. If the predicted results are not good, then the PLS model is re-trained and the new principal components are selected until the result is good.

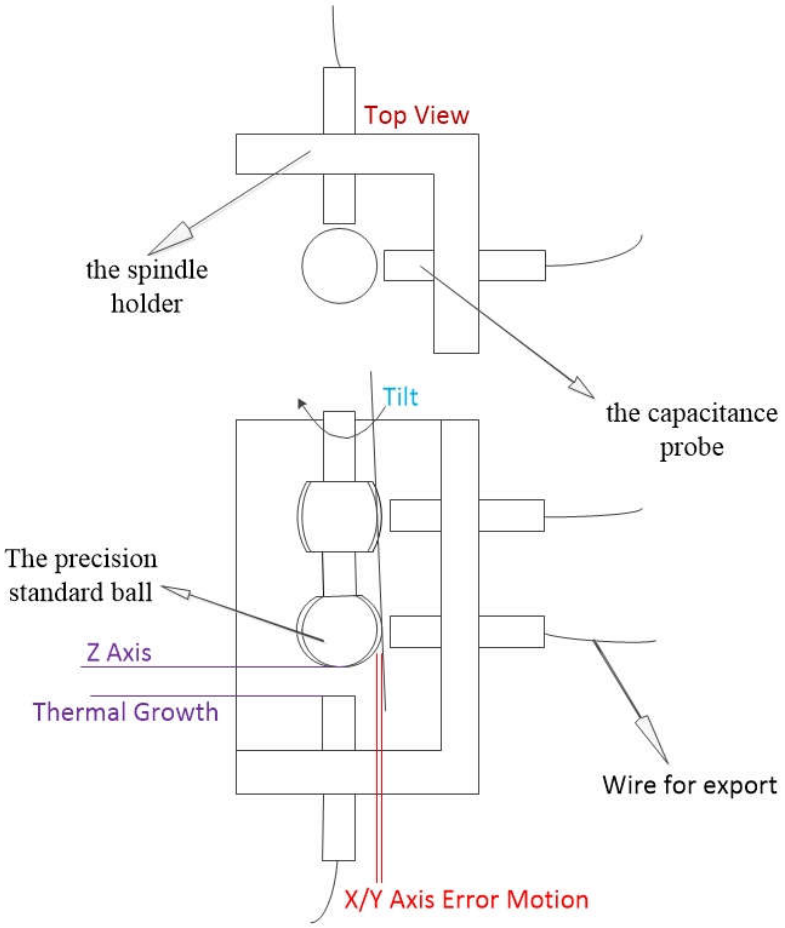

Figure 6. Displacement sensor position.

6. Thermal deformation experiment and result analysis

6.1. Experiment introduction

The experiment used the Lion Precision's spindle rotation error analyser for thermal deformation measurement. The entire measurement system includes high-resolution capacitive displacement sensors, precision standard balls, adjustable probe holders, and data acquisition components. The capacitive sensor driver has a resolution of up to 0.4 nanometers, which provides the most accurate spindle thermal deformation measurement. The precision standard ball is mounted on the spindle holder, the dynamic displacement of the standard ball is measured by the capacitance probe, and the data of each capacitive displacement sensor are combined and analysed to obtain the measurement result of thermal deformation. The displacement sensor installation position is shown in figure 6. A capacitive probe is installed on the bottom of the spindle to measure the axial Z-axis movement. A pair of right-angled capacitive probes is mounted on top of the precision standard balls to measure the radial X-axis and Y-axis movements.

A total of 7 temperature measurement points are arranged on the spindle to obtain the temperature field of the spindle. The Elite series TMP190 temperature sensor module is used. The position of the temperature measurement point is shown in table 4.

Table 4. Temperature sensor location.

No.	**Measuring position**
1	Spindle base
2	Spindle shaft head
3	Spindle housing middle
4	Spindle housing near front spindle bearing right side
5	Spindle housing near front spindle bearing left side
6	Spindle housing near rear spindle bearing right side
7	Spindle housing near rear spindle bearing left side

Considering that the temperature field and the thermal deformation are different at different rotational speeds, different spindle speed experiments are designed. The machine speed range is 2,000-12,000 *r/min*. In each set of fixed speed experiments, under the condition that the main shaft is fully lubricated and the cool system is turned on, the rotation speed is set until it reaches the thermal steady state

The laser sensor can achieve non-contact measurement of a measuring distance between 20mm.

Figure 7. TC series of multi-channel temperature tester.

Figure 8. LK-G5000 CMOS laser sensor.

The principle of diffuse reflection is used for laser acquisition. The wavelength of the light source is 655 ηm and the diameter of the laser light is 50 μm. Select LK-G5000 high-accuracy CMOS laser sensor, TC series multi-channel temperature tester and seven temperature sensors to measure the thermal deformation and temperature rise of the spindle (see figures 7 and 8).

Experimental measurement conditions: room temperature 25 °C, using progressive speed. The temperature field data and spindle thermal distortion data at different rotation speeds are measured when the spindle is unloaded. The spindle speed starts from low speed and continuously increases the spindle speed. Keep running at a required speed until the relative stability of the heat balance and thermal displacement is reached at this speed. By comparing the thermal displacement of the motor spindle with the temperature rise and the simulation, the correctness of the simulation result is verified, and the experimental basis can be provided for further calculation of the thermal error.

6.2. Model simulation and verification

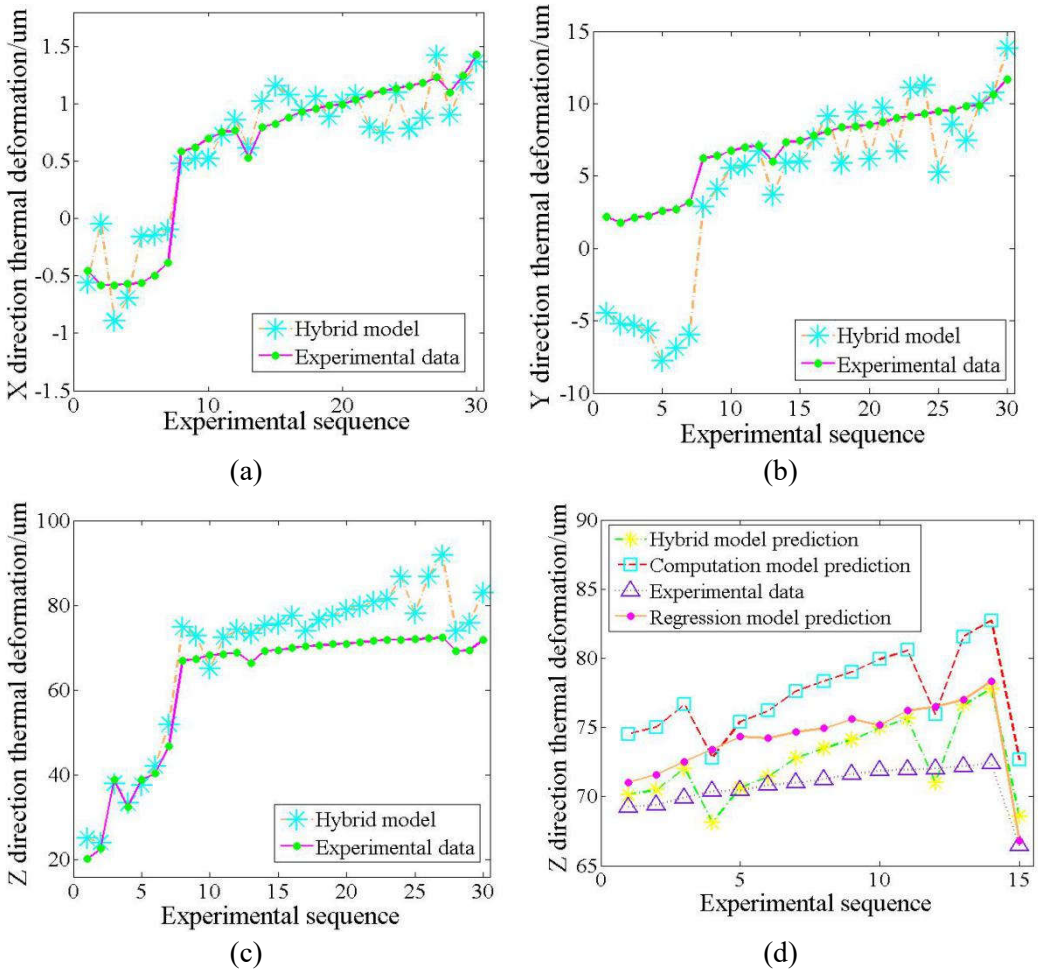

Figure 9. Hybrid modelling thermal deformation prediction results and comparison with other models in Z-direction. (a) Comparison between predicted X-direction thermal deformation and experimental data. (b) Comparison between predicted and experimental data of thermal deformation in Y direction. (c) Comparison between predicted and experimental data of thermal deformation in Z direction. (d) Comparison of the Z-direction thermal deformation hybrid model with other models.

This experiment measured the thermal deformation at different speeds from 2000-12,000 *r/min* and recorded the temperature rise at different speeds. A total of 50 sets of data were measured in the hybrid model results. 20 sets of data were used to establish a hybrid model, and the remaining 30 sets of data were used to test the accuracy of the hybrid model and the individual models. 15 sets of data were within the scope of model building data (internal data). The other 15 groups were outside the scope of the modelling data (external data).

Figure 9 (a), (b), (c) shows the overall prediction effect of the hybrid model in the three directions of X, Y, Z thermal deformation of the motorized spindle. It can be seen from the figure that the predicted thermal deformation of the hybrid model fluctuates within a certain range of experimental data, and the overall trend is similar to the experimental data. By calculation, the maximum prediction error in X direction is 0.6598 *um*, the minimum error is 0.1026 *um*, the maximum error in Y direction is 10.3142 *um*, the minimum error is 1.2752 *um*, the maximum error in Z direction thermal deformation prediction is 11.0347 *um*, and the minimum error is 0.8409 *um*.

The fitting curves of the predicted values and experimental data of each model of external data are shown in figure 9 (d). Since the thermal deformation in the Z direction is the largest, only the prediction of each model in the Z direction is shown, the other directions being similar to the Z direction. It can be seen from the figure that compared with the predicted value obtained by using the computation model and regression model alone, the predicted value of the hybrid prediction model corresponds better with the experimental data, and the error of the computation model is controlled between 6.433-11.725*um*. The prediction error of the regression model is controlled between 3.534-7.245*um*, and the prediction error of the hybrid modelling is within 2.312-6.356*um*. It can be seen from the figure that the hybrid model obtains higher prediction accuracy because the disadvantages of larger errors of the computation model are compensated by the PLS modelling method. The prediction results of the hybrid modelling can effectively follow the changing trend of the thermal deformation of the motorized spindle, basically around the experimental data distribution. The regression modelling and the computation modelling have large deviations from the experimental data and the error of the computation model is the largest. The hybrid modelling has higher prediction accuracy and improves the prediction accuracy. The data comparison results are shown in the table 5 below.

Table 5. Mean absolute error (MAE) of model predictions.

Model		Regression modelling	Hybrid modelling	Computation modelling
MAE	Internal data (X/Y/Z)	0.5396um /0.9107um/ 1.1321um	0.1443um /1.3016um /1.4885um	0.1773um /1.5479um /3.7069um
	External data (X/Y/Z)	0.4528um /0.8443um /6.1225um	0.0938um /1.2437um /1.1549um	0.2256um /1.5532um /7.396um

By calculating the mean absolute error of the model, the internal and external data models are used to predict the effect of regression modelling, computation modelling and hybrid modelling. As can be seen from table 5, the hybrid model has not much effect on the internal and external data of the model. The mean value of the model prediction error is lower than that of the regression model. The overall prediction effect of the hybrid modelling is better. The PLS regression model has better prediction effect than the external data model in the prediction of the data, and there is a large difference in the Z axis. This is a limitation of the regression model modelling, and it has good prediction effect only within the scope of modelling data. By adding the theoretical model, the ductility of the model is enhanced, and the accuracy of thermal deformation prediction is improved.

7. Conclusions

In this paper, by means of the analysis of the advantages and disadvantages of the computation model and the regression model, a hybrid prediction model is proposed in order to improve the thermal deformation prediction of the motorized spindle and the following conclusions are obtained:

- the hybrid model can be used to analyse the thermal deformation of the motorized spindle within a large data range;
- the hybrid model combines the advantages of the computation model and the regression model, and hence achieves higher prediction accuracy;
- the hybrid model prediction is better than the computation model and the regression model; it is proved that the hybrid model can make up for the prediction error of other models, and make the real-time thermal deformation compensation be possible during operation.

Acknowledgments

This research is supported by General Project of Shenyang Jianzhu University（2017017）, Innovation Team Development Program of Ministry of Education (IRT_15R45), Science and Technology Project of Shenyang (F16-096-1-00).

References

[1] Wanli X, Xuebing Y, Lang L and Julong Y 2009 *J.Mech. Eng.* **45**1-18
[2] Zhu J 2008*Robust ThermalErrorModeling and Compensation for CNC MachineTools* (USA: Department of Mechanical Engineering/The University of Michigan) pp35-56
[3] Bryan J B 1990*Ann CIRP* **39** 645-56
[4] Weck M, Mckeown P, Bonse R and Herbst U 1995 *Ann. Manuf. Technol.* **44** 589-98
[5] Ramesh R, Mannan M A and Poo A N 2000 *Int. J. Mach. Tools Manuf***40** 1235-56
[6] Mayr J et al 2012 *CIRP Ann.Manuf. Technol.***61** 771–91
[7] Yang L, Wanhua Z, Shuhuai L, Jun N, Wenwu W and Bingheng L 2015 *Int. J. Mach. Tools Manuf* **95** 20-38
[8] Tseng P C andHo J L 2002 *Int. J. Adv. Manuf. Technol.* **19** 850-8
[9] Qianjian G, Hongmei W and Aijun L *J. Hebei Univ. Sci. Technol.* **36** 344-50
[10] Chunli L, Zhiyuan R and Emin L 2012 *J. Nanjing Univ. Sci. Technol.***36** 1021-5
[11] Chunli L, Zhiyuan R, Jun L and Ruicheng F 2011 *J. Xian Jiaotong Univ.* **45** 50-4
[12] Chibing H, Jing Y and Tingchuan L 2010 *Mach. Des. Manuf.* **12** 30-2
[13] Dongman Y, Yanhui H, Di W, Xiaojing L 2014 Appl. Mech. Mater. **556-562** 1170-3
[14] Shuangyi L, Chen C and Huijun Y 2011 *Manufa. Autom.* **34** 57-60
[15] Chi M, Jun Y,Liang Z, Xuesong M and Shi H2015 *Appl. Therm. Eng.* **86** 251-68
[16] Chunli L, Zhiyuan R, Jun Land Lina R 2012 *Adv. Mater. Res* **466-467** 961-5
[17] Chunli L, Zhiyuan R, Jun L and Jingfang F 2011 *Adv. Mater. Res* **291-294** 2991-4
[18] Weiqing L, Jianzhong J, Yazhou X and Zichen C 2008 *Comput. Integr. Manuf. Syst.* **14** 295-9
[19] Liangyu C, Dawei Z, Weiguo G, Xiangyang Q and Yu S 2011 *Adv. Mater. Res* **154-155** 1305-9
[20] Chunli L and Zhiyuan R2010*Adv. Mater. Res.* **129-131** 556-60
[21] Yufeng S, Wenxin Y, Deping L, Wufa L and Zhiyong D2013 *Modul Mach. Tool Autom. Manuf. Technol.* **1** 36-41
[22] Yi Z and Jianguo Y 2011 *J. Mech. Eng.* **47** 134-9
[23] Ke Z, Xiangnan M, Lixiu Z, Wenda Y and Yuhou W 2013 *Adv. Mater. Res.* **712-715** 1209-12
[24] Dongman Y, Yanhui H, Di W and Xiaojing Li 2014 *Appl. Mech. Mater.* **556-562** 1170-73
[25] Min Y, Di W, Peixin W and Xiaojing L 2012 *Appl. Mech. Mater.***155-156**273-7
[26] Chi M, Zhao L, Xuesong M and Jun Y Arch.2016 *Proc. Inst. Mech. Eng. Part C J. Mech. Eng. Sci.* (vols 203-210) pp 1989-96
[27] Yong L, Shengdong G and Zhaopeng H 2011 *Adv. Mater. Res.* **305** 340-3
[28] Shi H, Xuesong M, Jun Y and Tao T 2012 *J. Huazhong Univ. Sci. Technol.* **40** 26-30
[29] Guisong D, Feng Y, Yusheng Z, Jianguo Y 2014 *Mach. Tool Hydra.* **42** 9-13

[30] Xiaoling W, Yubing S, Yong L, Menghan L and Jianfeng W 2014 *J. Hebei Univ. Eng.* **31** 104-7
[31] Zhifeng L, Minghui P, Aiping Z 2015 *Int. J. Adv. Manuf. Technol*. **76** 1913-26